SOX9-COL9A3–dependent regulation of choroid plexus epithelial polarity governs blood–cerebrospinal fluid barrier integrity

Keng Ioi Vong[a], Tsz Ching Ma[a], Baiying Li[a], Thomas Chun Ning Leung[a,b], Wenyan Nong[a], Sai Ming Ngai[a,b,c], Jerome Ho Lam Hui[a,b], Liwen Jiang[a,b,d], and Kin Ming Kwan[a,b,d,1]

[a]School of Life Sciences, The Chinese University of Hong Kong, Hong Kong, People's Republic of China; [b]State Key Laboratory of Agrobiotechnology, The Chinese University of Hong Kong, Hong Kong, People's Republic of China; [c]AoE Centre for Genomic Studies on Plant-Environment Interaction for Sustainable Agriculture and Food Security, The Chinese University of Hong Kong, Hong Kong, People's Republic of China; and [d]Centre for Cell and Developmental Biology, The Chinese University of Hong Kong, Hong Kong, People's Republic of China

Edited by Jeremy Nathans, Johns Hopkins University School of Medicine, Baltimore, MD, and approved December 29, 2020 (received for review May 13, 2020)

The choroid plexus (CP) is an extensively vascularized neuroepithelial tissue that projects into the brain ventricles. The restriction of transepithelial transport across the CP establishes the blood–cerebrospinal fluid (CSF) barrier that is fundamental to the homeostatic regulation of the central nervous system microenvironment. However, the molecular mechanisms that control this process remain elusive. Here we show that the genetic ablation of *Sox9* in the hindbrain CP results in a hyperpermeable blood–CSF barrier that ultimately upsets the CSF electrolyte balance and alters CSF protein composition. Mechanistically, SOX9 is required for the transcriptional up-regulation of *Col9a3* in the CP epithelium. The reduction of *Col9a3* expression dramatically recapitulates the blood–CSF barrier defects of *Sox9* mutants. Loss of collagen IX severely disrupts the structural integrity of the epithelial basement membrane in the CP, leading to progressive loss of extracellular matrix components. Consequently, this perturbs the polarized microtubule dynamics required for correct orientation of apicobasal polarity and thereby impedes tight junction assembly in the CP epithelium. Our findings reveal a pivotal cascade of SOX9-dependent molecular events that is critical for construction of the blood–CSF barrier.

blood–cerebrospinal fluid barrier | choroid plexus | Sox9 | epithelial polarity | microtubules

In vertebrates, tight regulation of the brain extracellular microenvironment is fundamental to central nervous system (CNS) homeostasis (1, 2). While the blood–brain barrier formed by junctional components between vascular endothelial cells is well perceived to provide insulation to the CNS, the importance of the choroid plexus (CP) has been neglected (3). Present in every brain ventricle, the CP acts as a physical barrier at the interface of systemic circulation and cerebrospinal fluid (CSF). The CNS is vulnerable to almost all undesired molecules present in the CSF (4); hence, failure in forming the blood–CSF barrier at the CP will conceivably elicit deleterious consequences to CNS function. However, the molecular control of blood–CSF barrier permeability remains largely elusive.

The CP consists of an outer layer of cuboidal epithelial cells enveloping a dense capillary core. Because the CP microvasculature is highly fenestrated and highly permeable, it has been suggested that the tight junctions between adjoining CP epithelial cells are the decisive parameter that governs the transepithelial penetrance of molecules into the CSF (5). Consistent with this notion, loss of the tight junction component MPDZ was linked to elevated permeability of the CP and neonatal hydrocephalus caused by an overabundance of CSF proteins (6). Studies in *Drosophila* or cultured mammalian cells suggest that tight junction formation often relies on the intricate interplay among cell polarity modules that designate the site of junctional assembly (7). Therefore, the establishment of a functional blood–CSF barrier is associated with epithelial polarity commitment in the CP. However, the vast majority of our current knowledge of epithelial cell polarization comes from simple in vitro cell-based systems (8).

Mechanisms that regulate apicobasal polarity are often more complicated in vivo and remain poorly understood (9, 10). Interestingly, the polarized configuration of membrane proteins in the CP epithelium is apparently different than all other secretory epithelia, such as epithelia in kidney or intestine (11). For example, the "basolateral transporters," such as Na^+ K^+ ATPase, NKCC1, and NHE1, are localized exclusively to the apical domain in the CP epithelium. Therefore, understanding the molecular basis that underlies this atypical epithelial polarity in the CP is key to determining the mechanisms that regulate blood–CSF barrier permeability.

SOX9 is a member of the high-mobility group transcription factor family that plays diverse roles in development (12). In humans, *SOX9* mutations are commonly associated with congenital CNS anomalies, including ventriculomegaly and hydrocephalus, but the pathological mechanisms are unknown (13–15). Previous studies in mice suggest that *Sox9* is essential for cell fate specification and differentiation in the neuroepithelium of neocortex,

Significance

Tight regulation of the brain microenvironment is fundamental to proper neurologic function. The restriction of molecule entry into the central nervous system from the brain vascular endothelium has been well studied; however, far less is known about the molecular events that control permeability across the choroid plexus (CP) epithelium at the interface between the systemic circulation and cerebrospinal fluid (CSF). Our study establishes an essential role for SOX9 in the regulation of CP permeability. SOX9 induces the transcription of *Col9a3*, which mediates the microtubule dynamics necessary for orienting cell polarity and thereby assembling epithelial tight junctions. Our findings lay the groundwork for the manipulation of blood–CSF barrier permeability and expand our understanding of epithelial tissue integrity.

Author contributions: K.I.V., S.M.N., J.H.L.H., L.J., and K.M.K. designed research; K.I.V., T.C.M., B.L., T.C.N.L., and W.N. performed research; K.I.V., T.C.M., B.L., T.C.N.L., W.N., S.M.N., J.H.L.H., L.J., and K.M.K. analyzed data; and K.I.V. and K.M.K. wrote the paper.

The authors declare no competing interest.

This article is a PNAS Direct Submission.

[1]To whom correspondence may be addressed. Email: kmkwan@cuhk.edu.hk.

This article contains supporting information online at https://www.pnas.org/lookup/suppl/doi:10.1073/pnas.2009568118/-/DCSupplemental.

Published February 1, 2021.

retina, and spinal cord during embryogenesis (16–18). Here we reveal a role for SOX9 in the developing CNS as an essential regulator of blood–CSF barrier function. Our findings demonstrate a series of cellular defects following the ablation of *Sox9* in the CP epithelium that eventually results in CSF electrolyte imbalance and aberrant hyperpermeability of the blood–CSF barrier. Mechanistically, SOX9 regulates the synthesis of collagen IX, deprivation of which markedly increases the vulnerability of the basement membrane, leading to the progressive loss of extracellular matrix (ECM) components. This disrupts ECM–cytoskeleton interactions and consequently perturbs the polarized microtubule dynamics required for maintenance of epithelial apicobasal polarity. Our results thus unveil a model of SOX9-dependent ECM signals that lead to cytoskeleton rearrangement to reinforce the apicobasal polarity in the CP epithelium and thereby establish the functional blood–CSF barrier.

Results

SOX9 Is Required for Blood–CSF Barrier Integrity. SOX9 expression was detected in the hindbrain CP once it emerged from the roof plate and persisted throughout gestation (*SI Appendix*, Fig. S1*A*). Immunohistochemistry showed that SOX9 was expressed exclusively in the CP epithelium and not in the underlying stroma (*SI Appendix*, Fig. S1 *B* and *C*). This expression pattern made SOX9 a candidate molecule that governs the acquisition of blood–CSF barrier function. To derive CP epithelium-specific *Sox9* conditional knockout mice (hereinafter referred as *Sox9* CKO), we crossed mice harboring *Sox9* floxed alleles with a *Pax2-Cre* transgene that showed robust activity in the rhombomere (*r*)-1–derived hindbrain

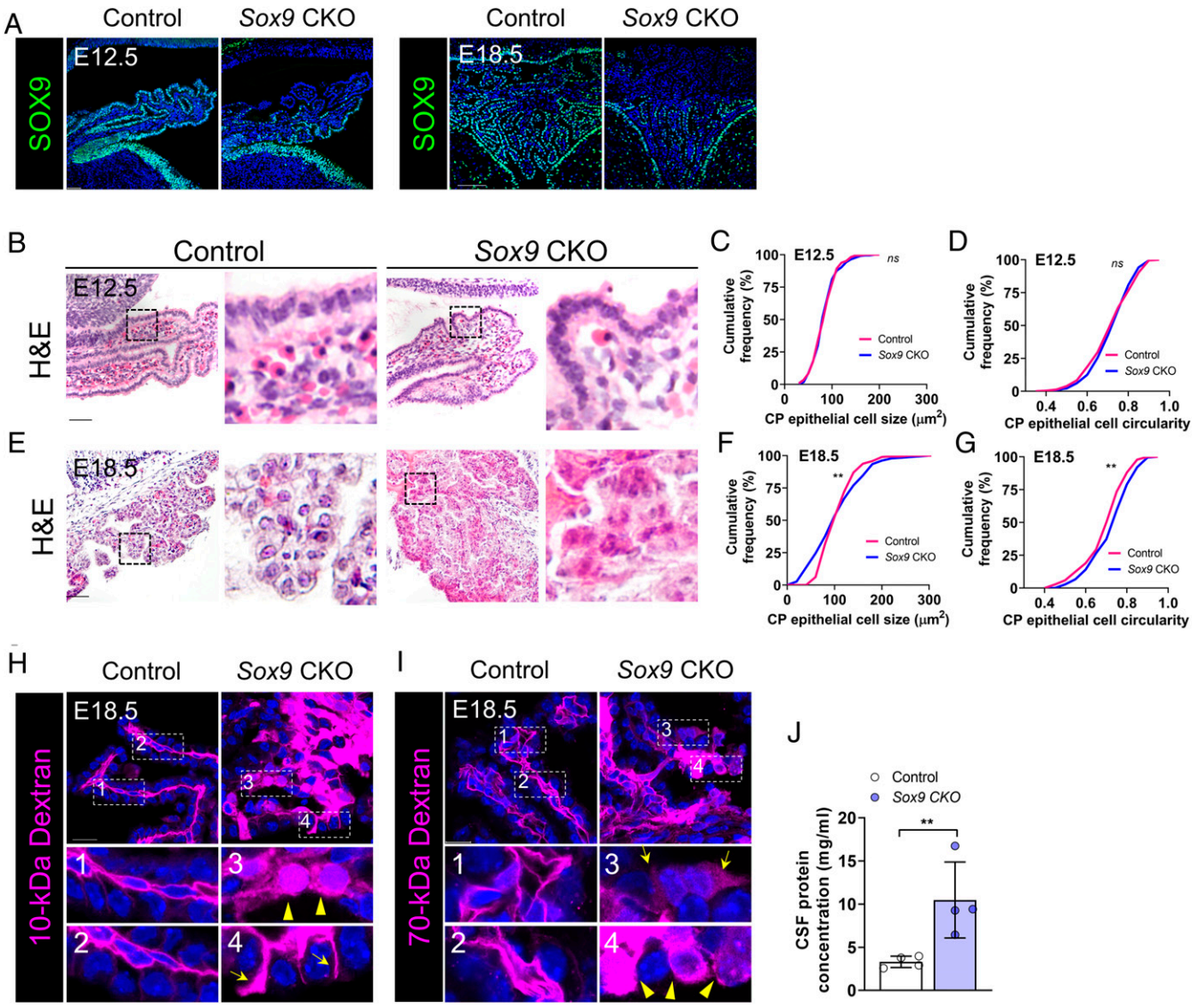

Fig. 1. Conditional inactivation of *Sox9* led to blood–CSF barrier dysfunction. (*A*) Representative images of coronal sections of E12.5 or E18.5 control and *Sox9* CKO immunostained for SOX9. $n = 3$ per genotype. (*B*–*G*) Representative histological images showing the cytoarchitecture of hindbrain CP of control and *Sox9* CKO at E12.5 (*B*) or E18.5 (*E*) and CP epithelial cell size and circularity at E12.5 (*C* and *D*) and E18.5 (*F* and *G*). $n \geq 150$ cells from three independent pairs of control and *Sox9* CKO, Kolmogorov–Smirnoff test. (*H* and *I*) Analysis of blood–CSF barrier permeability by in utero liver injection of rhodamine-conjugated 10-kDa dextran (*H*) or 70-kDa dextran (*I*) into E18.5 embryos. Loss of *Sox9* resulted in the penetration of both 10-kDa and 70-kDa dextran into the CP epithelial cell layer. Dextran was detected in the extracellular space between adjacent epithelial cells (arrows) or even taken up into the cytoplasm (filled arrowheads). $n = 3$ per genotype. (*J*) BCA protein assay analysis of protein abundance in CSF from E17.5 control and *Sox9* CKO. $n = 4$ per genotype. Data are mean ± SEM. $^{**}P < 0.01$; $^{***}P < 0.001$. (Scale bars: 50 μm in *A*; 100 μm in *B* and *E*; 20 μm in *H* and *I*.)

CP epithelium (*SI Appendix*, Fig. S2*A*). Immunohistochemistry confirmed the removal of SOX9 expression in the *Pax2-Cre* lineage of the CP (Fig. 1*A* and *SI Appendix*, Fig. S2*B*). Despite *Sox9* ablation, the epithelial morphology of the CP was comparable between control and *Sox9* CKO at E12.5 (Fig. 1 *B–D*). In situ hybridization indicated that *Transthyretin* (*Ttr*), a differentiation marker of CP epithelial cells, was expressed in the *Sox9*-deleted CP and maintained as development proceeded (*SI Appendix*, Fig. S3*A*). These results suggested that CP epithelial specification and differentiation were not perturbed by *Sox9* inactivation. However, histological examination of the *Sox9* CKO mutants at E18.5, which is the latest timepoint available for analysis due to perinatal lethality, revealed the absence of distinct frond-like folds projecting into the fourth ventricle (Fig. 1*E*). Moreover, analysis of cell size and shape indicated conspicuous morphometric irregularities of the *Sox9* CKO epithelium compared to controls (Fig. 1 *F* and *G*).

To investigate whether the aberrant cytoarchitecture hampers the integrity of the CP epithelium and abrogates blood–CSF barrier function, we delivered the albumin-binding azo dye Evans Blue into the circulation of *Sox9* CKO and control littermates by in utero injection into the fetal livers at E18.5. Evans Blue was confined within the vascular capillaries in control embryos but stained the brain parenchyma of *Sox9* CKO embryos (*SI Appendix*, Fig. S3*B*). To define the route of dextran leakage, we examined cross-sections of the brain following dye injection. Remarkably, the tracers extensively infiltrated the lateral intercellular space between adjoining CP epithelial cells or even permeated the entire cytoplasm in *Sox9* CKO mutants (*SI Appendix*, Fig. S3*B*).

To rule out the possibility that the albumin leakiness was due to an impairment of transport machineries, we also analyzed CP permeability using rhodamine-conjugated 10-kDa and 70-kDa dextran, which are inert polysaccharides. Consistent with our observations with Evans Blue, pronounced fluorescence was detected in the CP epithelial cells of *Sox9* CKO mutants, whereas the tracers were excluded from control CP epithelium (Fig. 1 *H–I*). Notably, the fluorescent dextran was not observed around the brain vasculature but instead was present in proximity to the ventricular surface in the *Sox9* CKO mutants (*SI Appendix*, Fig. S3 *C* and *D*). Immunofluorescent staining of vascular junction markers CD31 and Claudin-5 indicated that neither the vasculature in the brain nor that in the CP was affected by *Sox9* ablation (*SI Appendix*, Fig. S3 *E* and *F*). Moreover, the ultrastructure of the vascular endothelium appeared to be unaffected in *Sox9* CKO (*SI Appendix*, Fig. S3 *G* and *H*). These findings support the notion that tracer leakiness arises from a hyperpermeable CP epithelium and penetrates the neural tissues via the CSF in *Sox9* CKO mutants.

To corroborate this possibility, we measured the total protein concentration in the CSF using the bicinchonic acid (BCA) protein assay. Remarkably, the total protein abundance in the CSF was increased by more than 2-fold at E17.5 on *Sox9* ablation in the CP (Fig. 1*J*).

Loss of *Sox9* Perturbed CP Epithelial Apicobasal Polarity and Tight Junction Assembly. Because tight junctions are the key structures that restrict transepithelial permeability, we investigated whether the malfunction of the blood–CSF barrier in *Sox9* CKO mutants was accompanied by tight junction defects in the CP epithelium. For this purpose, we performed transmission electron microscopy (TEM) on E18.5 CP from control and *Sox9* CKO mutants. TEM demonstrated the typical tight junction ultrastructure in control CP at E18.5, which is characterized by linear electron-dense bands that form apical "kissing points" between apposing epithelial cells. Remarkably, the intercellular space between adjoining CP epithelial cells in *Sox9* CKO was substantially wider and without any electron-dense structures (Fig. 2*A*).

These observations suggest the absence of tight junctions between CP epithelia cells on *Sox9* ablation. Therefore, we examined the expression of the tight junction scaffold protein zonula occludens 1 (ZO-1) by immunohistochemistry. In control CP epithelial cells, ZO-1 was positioned at the apical-most surface. In sharp contrast, in the absence of SOX9, ZO-1 was dispersed broadly along the entire apicobasal axis (Fig. 2*B*). Polarized ZO-1 distribution depends on PAR protein complexes that specify the apical pole (19). Interestingly, PAR-3 failed to reach the apical region but instead mislocalized to the basolateral membrane in the CP epithelium of *Sox9* CKO mutants (Fig. 2*C*). In line with these observations, the adherens junction components E-cadherin and β-catenin were abnormally present on the apical cell surface in the mutants (Fig. 2 *D* and *E*). Interestingly, apicobasal polarity in *Sox9* CKO mutant CP epithelium was not disrupted until after E16.5 (*SI Appendix*, Fig. S4 *A–C*). These data suggest that SOX9 is required for the maintenance of correct apicobasal polarity in the CP epithelium.

Aberrant CP Epithelial Polarity Disrupts CSF Electrolyte Balance. To evaluate the impact of perturbations in apicobasal polarity, we first examined the directional transport system in the CP. Consistent with previous reports, by immunostaining of the Na^+ K^+ ATPase α1 subunit (ATP1A1), we showed that the Na^+/K^+ pump was positioned at the apical surface of the CP epithelium facing the brain ventricle. However, ATP1A1 was aberrantly diffused toward the basal side and colocalized with β-catenin in the *Sox9* CKO CP epithelium (Fig. 2*F* and *SI Appendix*, Fig. S4*D*). On the other hand, the basolateral transporter anion exchanger 2 protein (AE2) was displaced from the basal membrane and mislocalized to the apical domain following *Sox9* ablation (Fig. 2*G*). Although the overall abundance of ATP1A1 and AE2 appeared to be unaffected by the loss of *Sox9*, their availability at the apical membrane was substantially reduced in *Sox9* CKO (*SI Appendix*, Fig. S4*G*). Quantitative plots of transporter subcellular distribution across the apical-basal axis revealed sharp peaks of fluorescent signals corresponding to ATP1A1 and AE2 at the apical and basal poles, respectively, in controls. In contrast, the immunosignals of both apical and basal transporters were essentially uniform across the entire apicobasal axis in *Sox9* CKO mutants (Fig. 2 *H* and *I*). A similar phenomenon was observed with the water channel AQP1 and the $Na^+/K^+/2Cl^-$ cotransporter (NKCC1), suggesting the elimination of membrane transporter asymmetry (*SI Appendix*, Fig. S4 *E–H*).

Next, to investigate whether the loss of transporter polarization in CP impaired the homeostatic ionic balance, we measured the concentration of CSF electrolytes by atomic absorption spectroscopy. Although the level of K^+ in CSF was only subtly increased following *Sox9* deletion in CP, that of Na^+ ions was remarkably reduced, by 34%, in the *Sox9* CKO mutants (Fig. 2 *J* and *K*).

SOX9 Activates *Col9a3* Transcription for Collagen IX Synthesis. We sought to understand how SOX9 as a transcriptional regulator is able to influence the apicobasal polarity. In a search for molecular pathways bridging the loss of *Sox9* and polarity defects, we compared the transcriptome of E16.5 CP from control and *Sox9* CKO mice by performing RNA-sequencing. Interestingly, only a small set of genes were differentially expressed in the CP of *Sox9* CKO mutants (27 down-regulated and 13 up-regulated). The transcript levels of genes critical for establishing apicobasal polarity, including *aPKC*, *Crb3*, *Par-3, Scrib*, as well as major junctional complex members *Cldn1* and *ZO-1*, were not significantly altered by *Sox9* inactivation, as confirmed by RT-qPCR analyses (*SI Appendix*, Fig. S5 *A* and *B*). This implied that apicobasal polarity was not regulated by SOX9 at the transcriptional level, but instead that additional mechanisms are required for mediating SOX9 function. SOX9 often transcriptionally regulates multiple genes encoding ECM components in different organs (20), but, quite

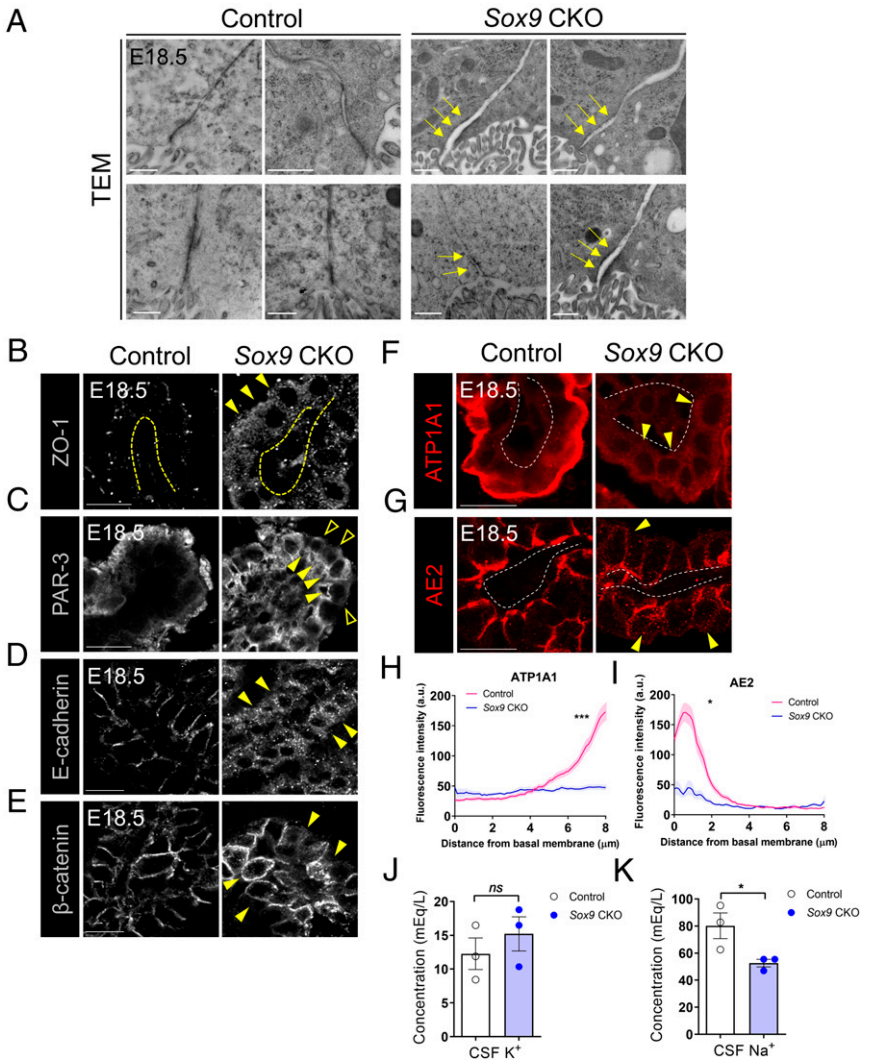

Fig. 2. *Sox9* is required for the assembly of tight junctions and establishment of correct epithelial polarity in the CP epithelium. (*A*) Representative electron micrographs of hindbrain CP epithelial cells from control and *Sox9* CKO at E18.5. Note the presence of electron-dense tight junction in controls but not in mutants (arrows). $n = 2$ per genotype. (*B*) Immunostaining analysis of ZO-1 subcellular localization. Yellow dotted lines outlined the basal membrane. $n = 3$ per genotype. (*C*) In the CP epithelium of *Sox9* CKO, PAR3 localization to the apical membrane was abolished (open arrowheads) but became detectable in the basal side (filled arrowheads). $n = 3$ per genotype. (*D* and *E*) In controls, E-cadherin and β-catenin were located predominantly on the basolateral membrane of CP epithelial cells but were mislocalized in *Sox9* CKO at E18.5 (filled arrowheads). $n = 3$ per genotype. (*F* and *G*) Representative images showing the distribution of Na^+/K^+ ATPase α1 subunit (ATP1A1) (*F*) and AE2 (*G*) in control and *Sox9* CKO. $n = 3$ per genotype. (*H* and *I*) Fluorescence intensity profile plots showing the subcellular distribution of ATP1A1 (*H*) and AE2 (*I*) along the apicobasal axis of individual CP epithelial cells. At least 30 cells from three independent litters were analyzed; multiple *t* tests. The shaded areas around the curves represent SEM. (*J* and *K*) Analysis of the concentrations of K^+ (*J*) and Na^+ ions (*K*) in CSF from E17.5 control and *Sox9* CKO by atomic mass spectrometry indicated a CSF electrolyte imbalance in the absence of *Sox9*. $n = 3$ per genotype. Data are mean ± SEM. $^*P < 0.05$; $^{***}P < 0.001$. (Scale bars: 500 nm in *A*, 20 μm in *B* and *C*, 10 μm in *D* to *G*.)

unexpectedly, loss of *Sox9* in the CP specifically abolished the expression of *Col9a2* and *Col9a3*, which encode the α2 and α3 chains of collagen IX, respectively (*SI Appendix*, Table S1). RT-qPCR analyses verified the dramatic down-regulation of *Col9a2* and *Col9a3* in *Sox9* CKO CP (Fig. 3 *A* and *C*).

To determine whether SOX9 directly binds to *Col9a2* and *Col9a3* loci in the CP, we performed in vivo chromatin immunoprecipitation (ChIP) with E16.5 wild-type CP. While SOX9 did not significantly associate with the *Col9a2* enhancer element, SOX9 displayed strong affinity to a dimeric consensus regulatory motif located within intron 1 of *Col9a3*. The same region was not pulled down by a nonspecific negative control IgG and SOX9 antibody did not preferentially immunoprecipitate a random region in the *Col9a3* 3′ UTR (Fig. 3 *B* and *D*). Meanwhile, previously reported SOX9 targets *Col2a1* and *Col4a2* were not regulated by SOX9 in the CP (*SI Appendix*, Fig. S5 *C* and *D*). Remarkably, *Col9a3* was expressed exclusively in the CP epithelium, as demonstrated by RNAscope in situ hybridization (*SI Appendix*, Fig. S6 *A* and *B*). *Col9a3* expression was completely abrogated from the majority of CP epithelial cells in the *Sox9* CKO mutants at both E14.5 and E18.5 (Fig. 3 *E* and *F*). Lineage tracing with the *ROSA26-YFP* reporter suggested that those few cells which express *Col9a3* were not descended from *Pax2-Cre*-labeled rhombomere 1 and thus are SOX9-positive (*SI Appendix*, Fig. S6*C*). Collectively, our results suggest that SOX9 physically binds to the *Col9a3* promoter and activates its transcription in the CP epithelium.

Collagen IX Is Essential for the Anchorage of ECM Macromolecules at the CP Subepithelial Basement Membrane. We proceeded to interrogate whether the loss of *Col9a3* has a causative linkage to

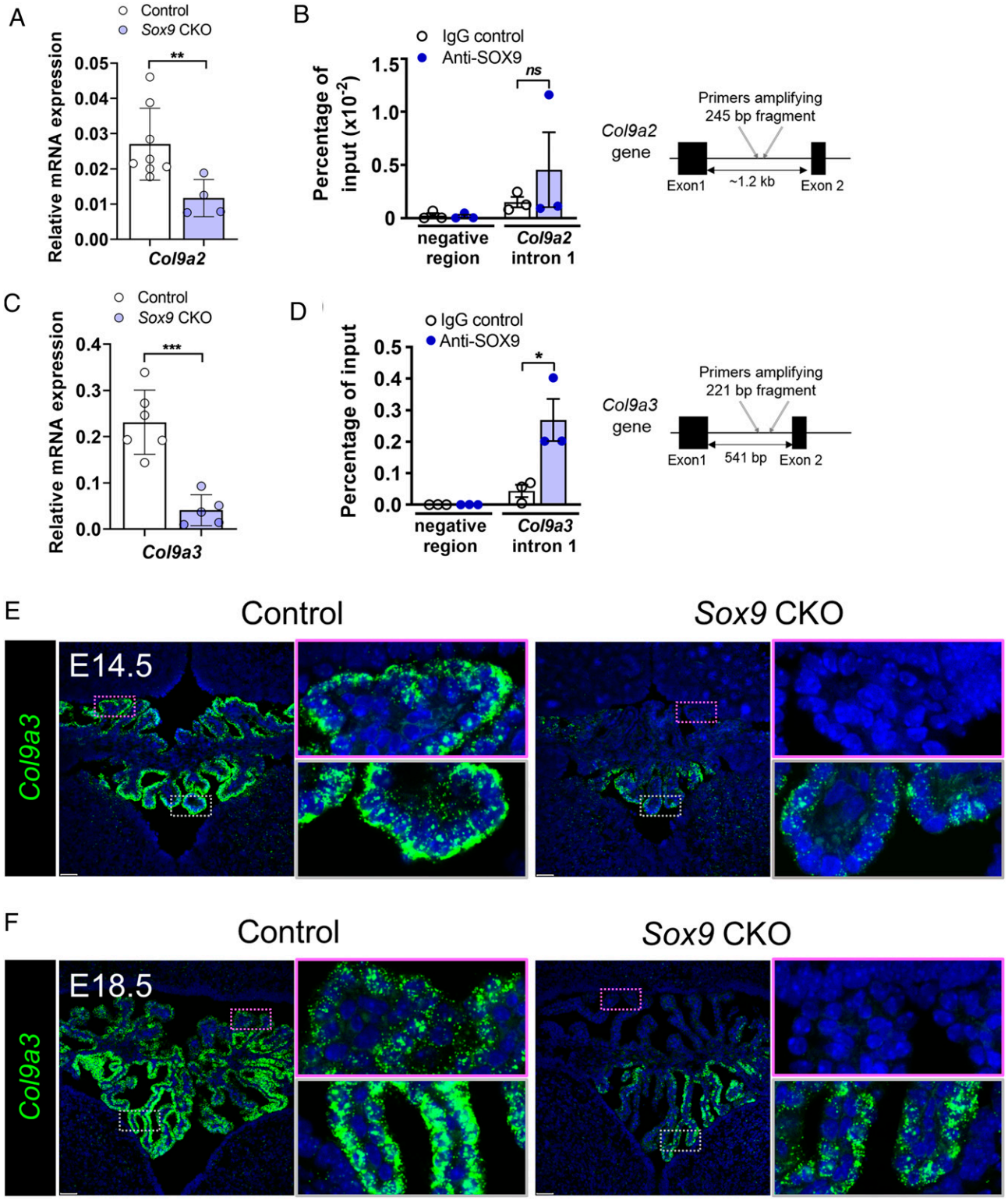

Fig. 3. SOX9 transcriptionally regulates *Col9a3* in CP epithelium. (*A*) RT-qPCR analysis of *Col9a2* expression level. $n = 4$ per genotype. (*B*) ChIP-qPCR analysis of SOX9 occupancy on putative binding motifs within intron 1 of *Col9a2*. Nontargeting IgG was used as a negative control. The binding occupancy is represented as % input. $n = 3$ independent experiments. (*C*) RT-qPCR analysis of *Col9a3* transcript level. $n = 5$ per genotype. (*D*) ChIP-qPCR analysis of SOX9 binding to intron 1 of *Col9a3*. $n = 3$ independent experiments. Data are mean ± SEM. $^*P < 0.05$; $^{**}P < 0.01$; $^{***}P < 0.001$. *ns*, not significant. (*E* and *F*) RNAscope showing the loss of *Col9a3* from CP epithelium in *Sox9* CKO at E14.5 (*E*) and E18.5 (*F*). $n = 3$ per genotype. (Scale bars: 100 μm in *E* and *F*.)

CP hyperpermeability in *Sox9* CKO mutants. To this end, we performed in utero electroporation to deliver siRNA against *Col9a3* into the hindbrain CP of wild-type embryos at E14.5, before establishment of the blood–CSF barrier (*SI Appendix*, Fig. S7*A*). Following electroporation, *Col9a3* expression levels were significantly reduced, as shown by RT-qPCR analyses (*SI Appendix*,

Fig. S7*B*) and RNAscope (*SI Appendix*, Fig. S7*C*). Silencing *Col9a3* expression caused the tight junction scaffold protein ZO-1 to become randomly scattered in the cytoplasm (Fig. 4*A* and *SI Appendix*, Fig. S7*D*), showing striking resemblance to the phenotypes of *Sox9* CKO mutants. Evaluation of CP permeability by tracer extravasation assay demonstrated that the CP epithelium was extensively infiltrated by 10-kDa or 70-kDa dextran on *Col9a3* silencing, although to a milder extent compared to that in *Sox9* CKO mutants (Fig. 4 *B* and *C*). In agreement with the CP hyperpermeability observed, *Col9a3* knockdown (KD) increased the total protein abundance in CSF by 42% (Fig. 4*D*). Like in the *Sox9* CKO, the apicobasal polarity was lost in the *Col9a3* KD CP epithelium (Fig. 4*E*). Correspondingly, neither the apical transporter ATP1A1 nor the basal transporter AE2 was correctly targeted to their respective membrane domains on *Col9a3* KD (Fig. 4 *F–I*). Moreover, Na^+ concentration in the CSF dropped significantly following *Col9a3* KD in the CP (*SI Appendix*, Fig. S7 *E* and *F*).

The remarkable recapitulation of the CP cellular defects in *Sox9* CKO mutants by silencing *Col9a3* expression prompted us to question further how the reduction of collagen IX would compromise blood–CSF barrier integrity. Previous studies reported that *Col9a3* is responsible for maintaining matrix integrity in cartilage by anchoring ECM macromolecules (21–23). In the CP, laminin was deposited as a discrete continuous border of the basement membrane underlying the epithelia. Despite early ablation of *Sox9* activity and down-regulation of *Col9a3* since the emergence of CP, laminin expression was initially normal in the basement membrane of *Sox9* CKO and did not become substantially altered until E16.5 (*SI Appendix*, S8 *A*, *C*, and *E*). Examination of collagen I deposition in the *Sox9* mutant CP across this temporal window led to similar observations, suggesting that the progressive displacement of ECM proteins from the basement membrane was not limited to specific matrix components (*SI Appendix*, Fig. S8 *B*, *D*, *F*, and *G*). Importantly, similar to what was observed in *Sox9* CKO mutants, only scattered and discontinuous patches of laminin deposition were detected in the CP 3 d after the KD of *Col9a3* (Fig. 4 *J* and *K*). These findings together suggest that the loss of collagen IX exasperated the structural integrity of CP epithelial basement membrane and resulted in the progressive elimination of ECM molecules. Interestingly, the destabilization of ECM molecules temporally precedes the disruption of apicobasal polarity in the *Sox9* CKO mutants, suggesting that deprivation of ECM molecules leads to disruption of apicobasal polarity (Fig. 2 *D* and *E* and *SI Appendix*, Fig. S4 *D–F*). Furthermore, the epithelium-specific laminin receptor integrin α6 was markedly obliterated from the basal membrane of both *Col9a3* KD and *Sox9* CKO CP (*SI Appendix*, Fig. S9 *A* and *B*). Therefore, we sought to directly demonstrate the effect of blocking integrin-ECM communication on cell polarity. Specifically, CP primary epithelial cells were incubated with normal IgG or function-blocking antibody against integrin α6 prior to seeding onto a laminin-coated surface. ZO-1 and β-catenin colocalized together at the cell-cell boundaries in control experiments, whereas interruption of integrin α6 binding to laminin caused the mislocalization of both proteins (*SI Appendix*, Fig. S9*C*). Thus, our results pinpoint the importance of integrin-ECM interactions in the regulation of epithelial polarity in the CP.

Collagen IX-Dependent ECM Signals Mediate Microtubule Dynamics Necessary for the Maintenance of Apicobasal Polarity in the CP Epithelium. Given that previous in vitro studies demonstrated that integrin-ECM communication may provide extrinsic cues for cytoskeleton remodeling necessary for epithelial polarity (24, 25), we first examined whether the loss of *Sox9* or the silencing of *Col9a3* would perturb the polarized cytoskeletal organization. Phalloidin staining indicated that the actin filaments were concentrated apically in the CP epithelium of both control and *Sox9* CKO mutants (Fig. 5*A*). In contrast, the acetylated tubulin became broadly distributed without clear nucleation origins on *Sox9* ablation (Fig. 5*B*). Notably, similar disruption of microtubule organization was observed following KD of *Col9a3* (Fig. 5*C*). We hypothesized that this atypical cytoskeletal polarity may reflect perturbations in microtubule dynamics. To evaluate this hypothesis, we performed ex vivo microtubule regrowth assay with CP tissues isolated from E17.5 control and *Sox9* CKO mice. In control CP epithelial cells, nascent microtubules focally emanated from the apex and displayed a typical astral configuration. In stark contrast, nascent microtubules were randomly nucleated in the cytoplasm of *Sox9* CKO epithelia (Fig. 5*D*). Quantification of α-tubulin fluorescence intensity showed that the number of nascent microtubules per unit area was significantly reduced in *Sox9* CKO CP epithelial cells (Fig. 5*E*). Moreover, we repeated the same experiments with *Col9a3* KD CP. Like what we observed in *Sox9*-deleted cells, following the silencing of *Col9a3*, nascent microtubules did not nucleate apically but instead emerged from widespread regions within the CP epithelial cells (Fig. 5 *F* and *G*). Because the typical array of noncentrosomal microtubules aligned along the apical-to-basal axis of epithelial cells is derived from the Golgi apparatus (26), we questioned whether the dispersed nucleation of microtubules was due to aberrant Golgi positioning. In the control CP epithelium, Golgi complexes were positioned in the apical cortex above the nucleus. A wind rose diagram illustrates that the Golgi was most frequently found at <30° to a reference line drawn parallel to the apicobasal axis (Fig. 5 *H* and *I*). In stark contrast, the apical positioning of the Golgi was lost and became randomly oriented to the basal or lateral side in the *Sox9* CKO CP epithelial cells (Fig. 5 *J* and *K*). These findings suggest that basement membrane-derived extrinsic cues are crucial for maintaining proper Golgi orientation and the polarized microtubule scaffold in CP epithelial cells.

In light of these findings, we examined the possibility that SOX9-dependent phenotypes were elicited by non–cell-autonomous ECM deficiency. Using the *ROSA26-YFP* reporter mice as an indicator for *Pax2-Cre* mosaicism in the CP, we found that laminin was abolished not only from the YFP^+ cells, but also from cells that were YFP^- and thus presumably $SOX9^+$ (*SI Appendix*, Fig. S10*A*). Likewise, the asymmetry of apical/basal transporters was impaired in *Sox9* CKO irrespective of YFP reporter expression (*SI Appendix*, Fig. S10*B*). Indeed, the aberrant transporter polarity was evident in some of the *Sox9* CKO cells that expressed *Col9a3* transcripts (*SI Appendix*, Fig. S10*C*). Together, these observations imply that the apicobasal polarity was regulated by SOX9 in a non–cell-autonomous manner.

***Sox9* Deletion in the CP Altered CSF Protein Composition.** To investigate whether these cellular defects disturbed CSF composition, we compared the proteome of CSF obtained from control and *Sox9* CKO mice by liquid chromatography-tandem mass spectrometry (LC-MS/MS). Interestingly, our results indicated that the loss of *Sox9* substantially altered the CSF protein composition (Fig. 6*A* and *SI Appendix*, Fig. S11 *A–D* and Table S2). To identify the key biological processes and pathways that are affected, we performed functional annotation clustering and Gene Ontology (GO) enrichment analysis for the three GO categories—biological processes (BP), cellular components (CC), and molecular functions (MF)—using Database for Annotation Visualization and Integrated Discovery (DAVID) (Fig. 6*B*). The key GO terms significantly enriched in BP, MF, and CC are protein folding, RNA binding, and extracellular exosomes, respectively.

Since exosomes are involved in the long-range delivery of signaling molecules, we assessed how this may impact the role of CSF as the signaling niche for CNS development. To this end, we tested the proliferative response of neural progenitors to CSF from wild-type mice or *Sox9* CKO mutants. While adding control CSF to neural progenitors of cerebellum suppressed their proliferation,

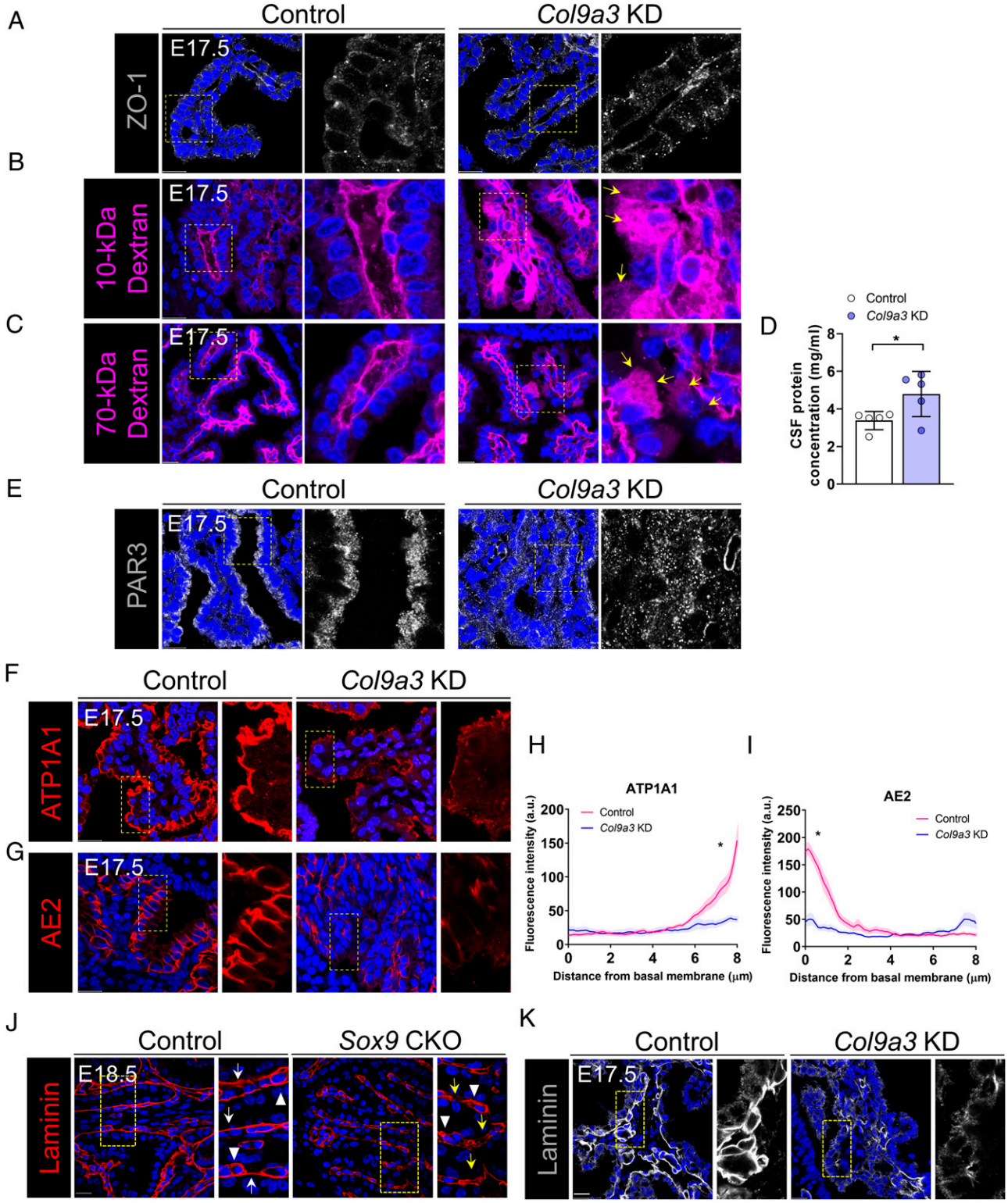

Fig. 4. Knockdown of *Col9a3* in the hindbrain CP epithelium. (*A*) Immunostaining analysis revealing the loss of apical localization of ZO-1 on *Col9a3* KD. $n = 3$ per genotype. (*B* and *C*) Representative images of CP showing the distribution of 10-kDa dextran (*B*) and 70-kDa dextran (*C*) in control and *Col9a3* KD embryos. $n = 3$ independent experiments. (*D*) Analysis of CSF protein content in control and *Col9a3* KD mice by BCA assay. Data are mean ± SEM. $^*P < 0.05$. (*E*) Immunostaining of PAR3 revealed CP epithelial cells failed to maintain apicobasal polarity following *Col9a3* KD. $n = 3$ independent experiments. (*F* and *G*) Representative images demonstrating the alteration of ATP1A1 (*F*) and AE2 (*G*) subcellular localization in *Col9a3* KD epithelial cells. (*H* and *I*) Plots of signal intensity of ATP1A1 (*H*) and AE2 (*I*) along the apicobasal axis of individual CP epithelial cells in control and *Col9a3* KD embryos. At least 30 cells from three independent experiments were analyzed; multiple *t* tests. Shaded area around the curves represents SEM. $^*P < 0.05$. (*J* and *K*) Immunostaining showed that the basal lamina of the CP epithelium was deprived of laminin following genetic ablation of *Sox9* (yellow arrows) (*J*) or *Col9a3* KD (*K*). White arrows and filled arrowheads indicate laminin expression at the subepithelial basement membrane and the vascular endothelium, respectively. $n = 3$ independent experiments or per genotype. (Scale bars: 20 μm in *A*–*C*, *E*–*G*, *J*, and *K*.)

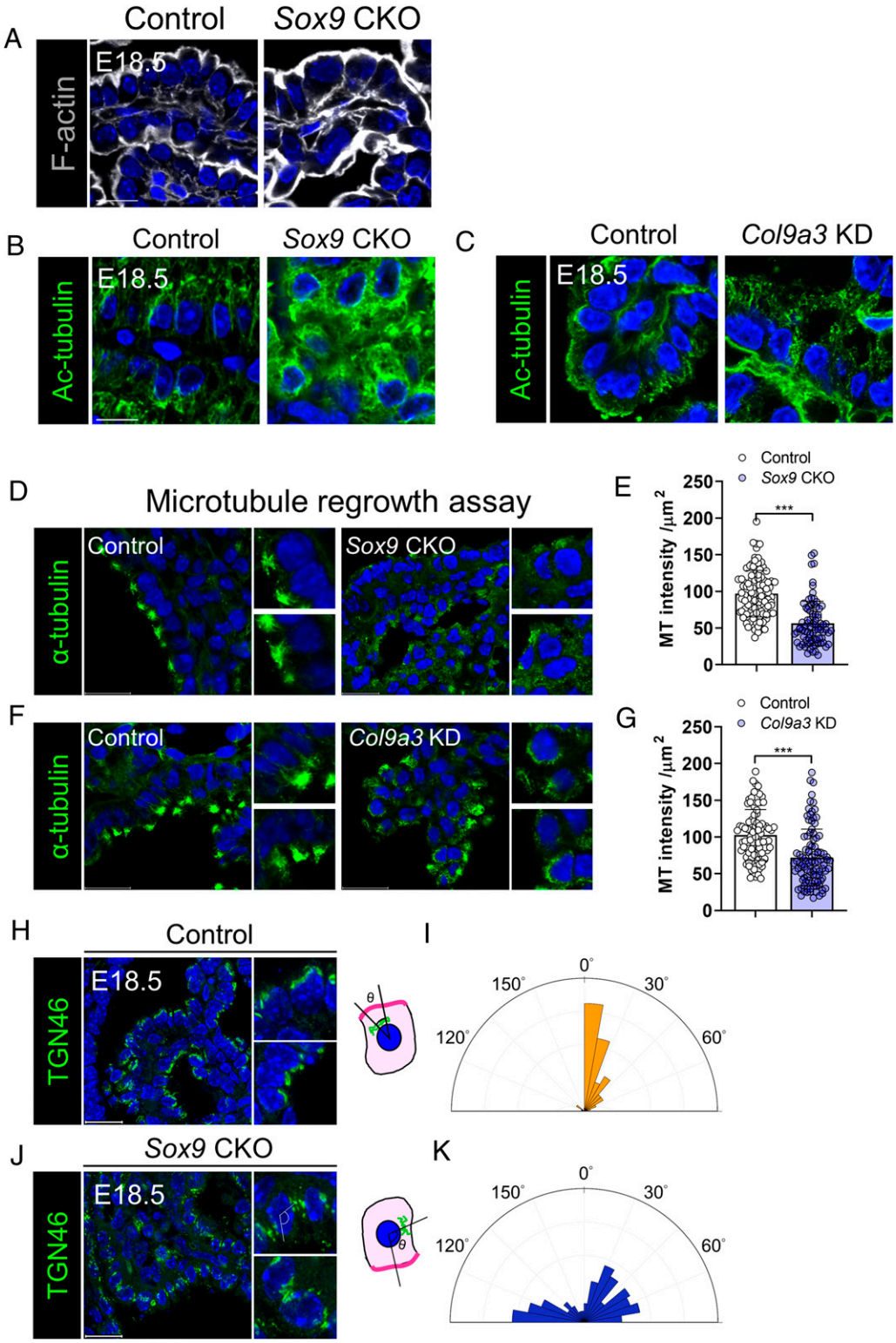

Fig. 5. Disruption of polarized microtubule scaffold by loss of *Sox9*. (*A*) Representative images of phalloidin staining demonstrating similar F-actin distribution in CP of control and *Sox9* CKO. (*B* and *C*) Examination of microtubule organization in the CP epithelium of E17.5 control and *Sox9* CKO (*B*) or *Col9a3* KD embryos (*C*) by immunostaining for acetylated tubulin (Ac-tubulin). (*D*–*G*) Microtubule regrowth assay showing that nascent microtubules were focally emanated from the apical domain in normal CP epithelial cells. (*D*) Conditional *Sox9* deletion or (*F*) the KD of *Col9a3* led to aberrant nucleation of MTs from multiple loci in the cytoplasm. $n = 3$ per group. Quantification of α-tubulin intensity indicates reduced microtubule nucleation in *Sox9* CKO (*E*) or *Col9a3* KD CP (*G*). $n = 150$ cells. (*H*–*K*) Analysis of Golgi orientation in CP epithelium by immunostaining for TGN46 in controls (*H*) and *Sox9* CKO mutants (*J*). Wind rose diagram showing the orientation of Golgi apparatus to a reference line drawn parallel to the apicobasal axis and across the nucleus in controls (*I*) and *Sox9* CKO mutants (*K*). $n = 150$ cells. $^{***}P < 0.001$. (Scale bars: 50 μm in *A*; 10 μm in *B* and *C*; 20 μm in *D*, *F*, *H*, and *J*.)

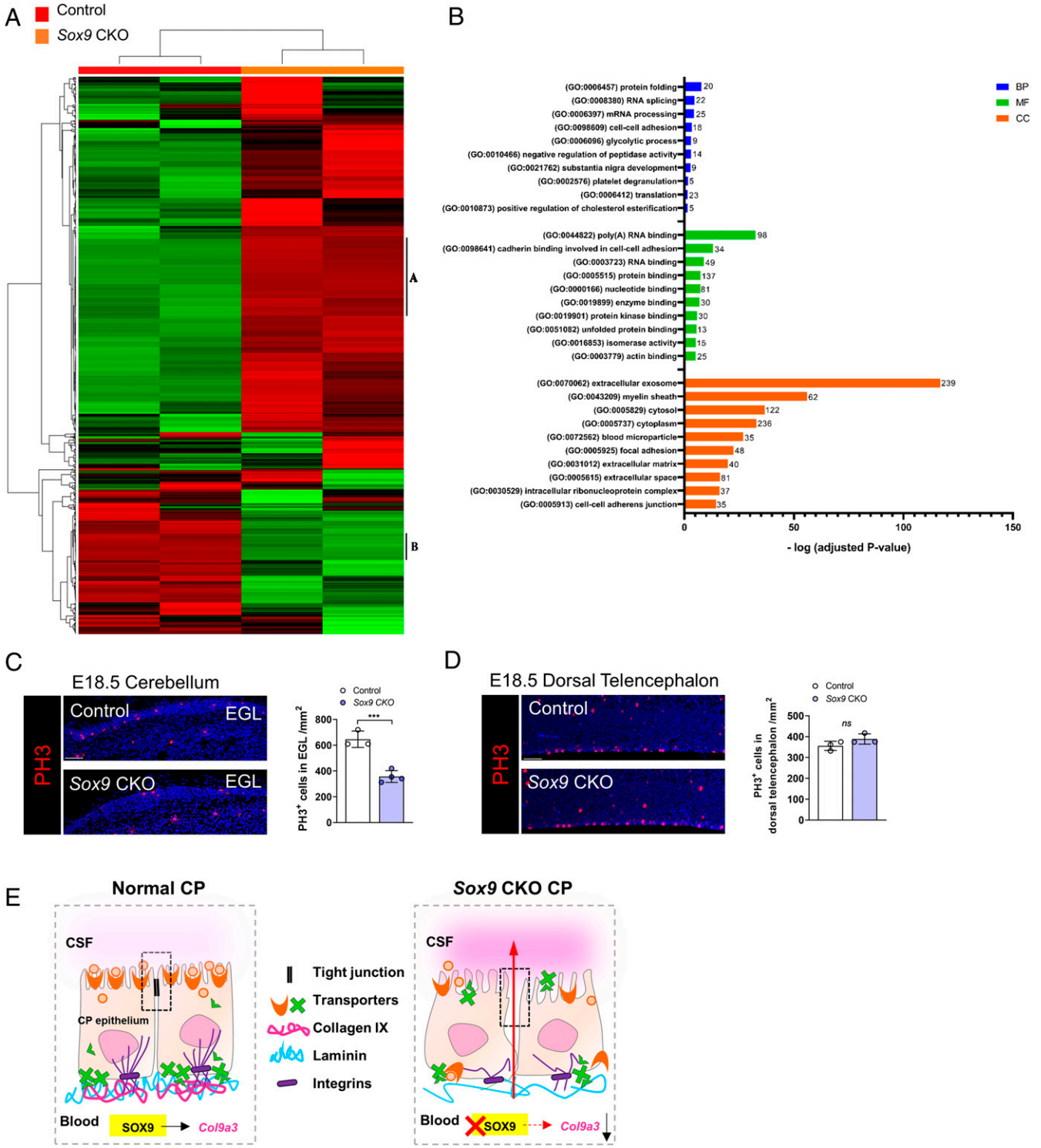

Fig. 6. Removal of *Sox9* from CP altered CSF protein composition. (*A*) Quantitative analysis of proteins in CSF from control or *Sox9* CKO by LC-MS/MS. CSF protein composition represents pooled samples from at least three mice per genotype. Hierarchical clustering was performed using the average linkage clustering method and the Pearson metric with Proteome Discoverer. Proteins enriched in CSF of *Sox9* CKO or control are indicated in regions A and B, respectively. (*B*) The differentially expressed proteins were subjected to analysis with DAVID for annotation enrichment analysis. The 10 most significantly enriched GO terms in BP, MF, and CC terms are presented. All the Benjamini- adjusted *P* values of the terms were negative 10-based log-transformed. (*C* and *D*) Immunostaining for PH3 and quantification of $PH3^+$ cells in the cerebellar external granular layer (EGL) (*C*) and dorsal telencephalon (*D*) of control and *Sox9* CKO. At least eight sections from each embryo were analyzed. $n = 3$ per genotype. (Scale bars: 20 μm.) (*E*) Schematic diagram of the proposed working model of SOX9 in the regulation of blood–CSF barrier function. Data are mean ± SEM. $***P < 0.001$. ns, not statistically significant.

CSF isolated from *Sox9* CKO constrained progenitor expansion to a markedly greater extent (*SI Appendix*, Fig. S11*E*). However, neither CSF from controls nor CSF from *Sox9* CKO mice produced a significant effect on progenitors isolated from the developing neocortex (*SI Appendix*, Fig. S11*F*).

We further examined progenitor expansion in vivo by immunostaining for phospho-histone H3 (PH3), which labels cells undergoing mitosis. Interestingly, the number of $PH3^+$ cells in the external granular layer of cerebellum was decreased remarkably following *Sox9* ablation in the CP (Fig. 6*C*). As SOX9 is not expressed in granule cells, this difference was presumably due to alterations in the CSF proteome (26, 27). In contrast, the number of mitotic progenitors in the dorsal telencephalon appeared to be similar in control and *Sox9* CKO (Fig. 6*D*). These results suggest that inactivation of *Sox9* in the CP led to changes in the CSF environmental niche that ultimately altered neural progenitor behavior in a region-specific manner across different CNS compartments.

Discussion

The molecular pathways that regulate blood–CSF barrier permeability were previously unknown. Here we provide evidence that the maintenance of apicobasal polarity in the CP epithelium is fundamental to restricting transepithelial permeability and thus establishing the functional blood–CSF barrier. Mechanistically, SOX9 transcriptionally regulates the expression of *Col9a3*, which is required for the intricate interplay between ECM molecules and microtubule dynamics necessary for polarity orientation and tight junction assembly.

The correct apicobasal polarity of epithelial cells is the basis of organ function (28). Pioneering in vitro studies have implied an instrumental role of basement membrane ECM molecules in defining the apical versus basal pole of epithelium (25); however, the in vivo relevance of ECM signals to epithelial polarity has remained largely ambiguous and controversial (29, 30). Studies in *Caenorhabditis elegans* suggested that laminin deposition was required to specify the formation of an apical lumen in the pharynx but not in the intestine (31), while in the lung epithelium of developing mice, the abrogation of collagen II and laminin resulting from *Sox9* deletion did not cause abnormalities in epithelial polarity (32). Interestingly, we found that apicobasal polarity was almost immediately defined once the CP epithelium emerged from the neuroectodermal progenitors at E12. Remarkably, at this stage, the ECM proteins were just synthesized in the CP and barely deposited to the basement membrane. Therefore, it appears that the initial establishment of apicobasal polarity in the CP epithelium is independent of interactions with the ECM components but rather requires some inherent mechanisms. However, unexpectedly, this already defined epithelial polarity is disrupted by the down-regulation of *Col9a3* expression in the CP epithelium, presumably due to weakened anchorage of other matrix macromolecules. This disputes the common perception that the importance of ECM in epithelial polarity is restricted to scenarios when cells are not previously in contact with matrix proteins, such as during de novo lumen formation or tissue regeneration (10, 25). Once the basal pole is specified by contacts with the basement membrane, epithelial polarity is reinforced and maintained by intrinsic polarity modules, such as the PAR and Scribble protein complexes (9).

Intriguingly, our findings contrast with this conventional paradigm and emphasize the vital role of ECM-derived extrinsic cues in the homeostatic maintenance of epithelial polarity. We found that a lack of *Col9a3* disturbed proper Golgi orientation and impaired the polarized reassembly of microtubules, which conceivably altered the initially defined apicobasal polarity. Mechanisms driving the polarization of microtubule scaffolds in mammalian epithelium remain unclear (33). Whether such an ECM-dependent pathway is context-dependent or represents a generalized phenomenon in different epithelia of mammalian tissues is a topic for future investigation. Possible mechanisms by which microtubules aid the regulation of cell polarity include the generation of contractile forces that couple cell polarity to tissue architecture and control organelle polarity for directional cargo transport (34, 35); however, the role of microtubules in epithelial polarity regulation in mammalian tissues remains largely unclear.

We further demonstrate that the expression of *Col9a3* is under the regulation of SOX9. *Col9a3* was exclusively expressed in CP epithelium in the CNS. Since the cellular anomalies observed following KD of *Col9a3* are essentially phenocopies of *Sox9* CKO mutants, it is likely that the CP hyperpermeability defects are caused predominantly by a deficiency in collagen IX. This may explain the non–cell-autonomous SOX9 regulation of CP epithelial apicobasal polarity: although *Sox9* CKO mutants showed mosaicism of *Sox9* deletion in the CP epithelium, the deficits of collagen IX deposition in the basement membrane destabilized ECM molecules derived from both *Sox9*-deleted cells and the neighboring SOX9-expressing cells. Consequently, the epithelial polarity was globally disrupted in the mosaic *Sox9* CKO mutants.

SOX9 mutations in human neonates commonly manifest hydrocephalus accompanied by ventriculomegaly, but the mechanistic linkage is unclear (13–15). Hydrocephalus can be caused by dysfunction of ependymal cells lining the ventricles, impairment of CSF dynamics, or overabundance of CSF proteins (6, 36, 37). Therefore, the elevated levels of CSF proteins on loss of SOX9 function provides a possible explanation for the pathophysiology of hydrocephalus in human patients. Nevertheless, the perinatal lethality of *Sox9* CKO mice hinders further verification of such a premise. The CP has drawn increasing attention recently because of its ability to dynamically modulate CSF signaling niches for diverse purposes (38–43). Interestingly, the responses to CSF appeared to be heterogeneous across different compartments of the CNS. A previous study indicated significant differences in the transcriptome of CP from different brain ventricles, such that CSF composition is regionalized albeit with continuous CSF flow between brain ventricles (44). Our results suggest the likelihood that such region-specific CSF microenvironments is essential for exercising target-specific responses at the functional level.

Taken together, our findings suggest a model of blood–CSF barrier permeability regulation that depends on a SOX9-COL9A3-microtubule functional axis, which may lead to strategies that manipulate CP epithelial permeability or the dynamics of CSF composition for therapeutic and pharmacologic purposes.

Materials and Methods

Experimental Animals. *Pax2-Cre*, *Sox9*$^{fx/fx}$, and *R26R-YFP* mouse lines were described previously (45–47). *Pax2-Cre;Sox9*$^{fx/fx}$ mice are referred to as *Sox9* CKO. Mice with the *Pax2-Cre;Sox9*$^{fx/+}$ genotype were used as controls unless otherwise defined. All animal procedures were conducted with the approval of the Animal Experimentation Ethics Committee of The Chinese University of Hong Kong.

Blood–CSF Barrier Permeability Assay. In utero liver injection of tracers was performed as described previously (48). Timed-pregnant mice were anesthetized, and uterine horns were exposed. Fluorescent tracers (5 μL of 2 mg/mL 10-kDa or 70-kDa tetramethylrhodamine-conjugated dextran in PBS or 1% Evans Blue in PBS) were injected into the livers of embryos. Tracers were allowed to circulate for 10 min before sacrifice of the embryos.

In Utero Electroporation. Timed-pregnant ICR mice at E14.5 were anesthetized, and uterine horns were exposed. Then 1 μL of ON-TARGETPlus SMARTpool siRNA targeting *Col9a3* (50 nM) or siGLO nontargeting control (Dharmacon; GE Healthcare) was microinjected into the fourth ventricle with a fire-polished glass capillary connected to a micro syringe pump controller (Micro4; World Precision Instruments). To perform electroporation, five 50-ms pulses of 35 V at 950-ms intervals were delivered across the CP (ECM830; BTX).

Quantification and Statistical Analysis. The brightness and contrast of the confocal images were adjusted with Leica Application Suite X (LAS X; version 3.0.2.16120) or Olympus FV10-ASW (version 04.02.02.09). Fluorescence intensity and Golgi orientation were analyzed using Fiji/ImageJ version 1.43. All statistical analyses were performed using GraphPad Prism 8 software, and significance was accepted at $P < 0.05$. All images are representative of at least three independent experiments unless specified otherwise. Data analysis was not performed blinded to the mouse genotype, because the phenotype often could be obviously recognized.

Additional information of study methodology is provided in *SI Appendix, Materials and Methods*.

Data Availability. Transcriptome data have been deposited in the National Center for Biotechnology Information database through the BioSample submission portal (accession nos. SAMN16774154 and SAMN16774155). All other study data are included in the article and *SI Appendix*.

ACKNOWLEDGMENTS. We thank Richard R. Behringer (University of Texas MD Anderson Cancer Center) for providing the *Sox9* conditional mouse line, helpful advice, and comments on the manuscript. We also thank Sze-nim Lim and Freddie Kwok for their excellent technical support. The work described in this paper was supported by grants from the Research Grant Council of the Hong Kong Special Administrative Region (GRF 14105418, CRF 4012-16E, and AoE/M-05/12) and a Chinese University of Hong Kong Direct Grant for Research.

1. E. M. Rhea, W. A. Banks, Role of the blood-brain barrier in central nervous system insulin resistance. *Front. Neurosci.* **13**, 521 (2019).
2. R. M. Fame, M. K. Lehtinen, Emergence and developmental roles of the cerebrospinal fluid system. *Dev. Cell* **52**, 261–275 (2020).
3. M. P. Lun, E. S. Monuki, M. K. Lehtinen, Development and functions of the choroid plexus-cerebrospinal fluid system. *Nat. Rev. Neurosci.* **16**, 445–457 (2015).
4. N. R. Saunders, S. A. Liddelow, K. M. Dziegielewska, Barrier mechanisms in the developing brain. *Front. Pharmacol.* **3**, 46 (2012).
5. B. Engelhardt, L. Sorokin, The blood-brain and the blood-cerebrospinal fluid barriers: Function and dysfunction. *Semin. Immunopathol.* **31**, 497–511 (2009).
6. J. Yang *et al.*, Murine MPDZ-linked hydrocephalus is caused by hyperpermeability of the choroid plexus. *EMBO Mol. Med.* **11**, e9540 (2019).
7. X. Chen, I. G. Macara, Par-3 controls tight junction assembly through the Rac exchange factor Tiam1. *Nat. Cell Biol.* **7**, 262–269 (2005).
8. A. Manninen, Epithelial polarity—Generating and integrating signals from the ECM with integrins. *Exp. Cell Res.* **334**, 337–349 (2015).
9. E. Rodriguez-Boulan, I. G. Macara, Organization and execution of the epithelial polarity programme. *Nat. Rev. Mol. Cell Biol.* **15**, 225–242 (2014).
10. J. L. Lee, C. H. Streuli, Integrins and epithelial cell polarity. *J. Cell Sci.* **127**, 3217–3225 (2014).
11. H. H. Damkier, P. D. Brown, J. Praetorius, Cerebrospinal fluid secretion by the choroid plexus. *Physiol. Rev.* **93**, 1847–1892 (2013).
12. A. Jo *et al.*, The versatile functions of Sox9 in development, stem cells, and human diseases. *Genes Dis.* **1**, 149–161 (2014).
13. A. Matsumoto *et al.*, The presence of diminished white matter and corpus callosal thinning in a case with a SOX9 mutation. *Brain Dev.* **40**, 325–329 (2018).
14. P. Antwi *et al.*, A novel association of campomelic dysplasia and hydrocephalus with an unbalanced chromosomal translocation upstream of SOX9. *Cold Spring Harb. Mol. Case Stud.* **4**, a002766 (2018).
15. B. Gentilin *et al.*, Phenotype of five cases of prenatally diagnosed campomelic dysplasia harboring novel mutations of the SOX9 gene. *Ultrasound Obstet. Gynecol.* **36**, 315–323 (2010).
16. C. E. Scott *et al.*, SOX9 induces and maintains neural stem cells. *Nat. Neurosci.* **13**, 1181–1189 (2010).
17. R. A. Poché, Y. Furuta, M. C. Chaboissier, A. Schedl, R. R. Behringer, Sox9 is expressed in mouse multipotent retinal progenitor cells and functions in Müller glial cell development. *J. Comp. Neurol.* **510**, 237–250 (2008).
18. C. C. Stolt *et al.*, The Sox9 transcription factor determines glial fate choice in the developing spinal cord. *Genes Dev.* **17**, 1677–1689 (2003).
19. T. Hirose *et al.*, Involvement of ASIP/PAR-3 in the promotion of epithelial tight junction formation. *J. Cell Sci.* **115**, 2485–2495 (2002).
20. C. D. Oh *et al.*, SOX9 regulates multiple genes in chondrocytes, including genes encoding ECM proteins, ECM modification enzymes, receptors, and transporters. *PLoS One* **9**, e107577 (2014).
21. A. Hanson-Kahn *et al.*; University of Washington Center for Mendelian Genomics, Autosomal recessive stickler syndrome resulting from a COL9A3 mutation. *Am. J. Med. Genet. A.* **176**, 2887–2891 (2018).
22. K. Blumbach *et al.*, Combined role of type IX collagen and cartilage oligomeric matrix protein in cartilage matrix assembly: Cartilage oligomeric matrix protein counteracts type IX collagen-induced limitation of cartilage collagen fibril growth in mouse chondrocyte cultures. *Arthritis Rheum.* **60**, 3676–3685 (2009).
23. B. Brachvogel *et al.*, Comparative proteomic analysis of normal and collagen IX null mouse cartilage reveals altered extracellular matrix composition and novel components of the collagen IX interactome. *J. Biol. Chem.* **288**, 13481–13492 (2013).
24. L. E. O'Brien *et al.*, Rac1 orientates epithelial apical polarity through effects on basolateral laminin assembly. *Nat. Cell Biol.* **3**, 831–838 (2001).
25. M. A. Morrissey, D. R. Sherwood, An active role for basement membrane assembly and modification in tissue sculpting. *J. Cell Sci.* **128**, 1661–1668 (2015).
26. K. I. Vong, C. K. Leung, R. R. Behringer, K. M. Kwan, Sox9 is critical for suppression of neurogenesis but not initiation of gliogenesis in the cerebellum. *Mol. Brain* **8**, 25 (2015).
27. R. Hashimoto *et al.*, Origins of oligodendrocytes in the cerebellum, whose development is controlled by the transcription factor, Sox9. *Mech. Dev.* **140**, 25–40 (2016).
28. D. M. Bryant, K. E. Mostov, From cells to organs: Building polarized tissue. *Nat. Rev. Mol. Cell Biol.* **9**, 887–901 (2008).
29. F. Alpy *et al.*, Generation of a conditionally null allele of the laminin alpha1 gene. *Genesis* **43**, 59–70 (2005).
30. J. H. Miner, C. Li, J. L. Mudd, G. Go, A. E. Sutherland, Compositional and structural requirements for laminin and basement membranes during mouse embryo implantation and gastrulation. *Development* **131**, 2247–2256 (2004).
31. J. P. Rasmussen, S. S. Reddy, J. R. Priess, Laminin is required to orient epithelial polarity in the C. elegans pharynx. *Development* **139**, 2050–2060 (2012).
32. B. E. Rockich *et al.*, Sox9 plays multiple roles in the lung epithelium during branching morphogenesis. *Proc. Natl. Acad. Sci. U.S.A.* **110**, E4456–E4464 (2013).
33. N. Akhtar, C. H. Streuli, An integrin-ILK-microtubule network orients cell polarity and lumen formation in glandular epithelium. *Nat. Cell Biol.* **15**, 17–27 (2013).
34. S. E. Siegrist, C. Q. Doe, Microtubule-induced cortical cell polarity. *Genes Dev.* **21**, 483–496 (2007).
35. A. Singh *et al.*, Polarized microtubule dynamics directs cell mechanics and coordinates forces during epithelial morphogenesis. *Nat. Cell Biol.* **20**, 1126–1133 (2018).
36. R. Park *et al.*, Yap is required for ependymal integrity and is suppressed in LPA-induced hydrocephalus. *Nat. Commun.* **7**, 10329 (2016).
37. D. D. Limbrick Jr *et al.*, Cerebrospinal fluid biomarkers of infantile congenital hydrocephalus. *PLoS One* **12**, e0172353 (2017).
38. S. Balusu *et al.*, Identification of a novel mechanism of blood-brain communication during peripheral inflammation via choroid plexus-derived extracellular vesicles. *EMBO Mol. Med.* **8**, 1162–1183 (2016).
39. M. E. Coulter *et al.*, The ESCRT-III protein CHMP1A mediates secretion of sonic hedgehog on a distinctive subtype of extracellular vesicles. *Cell Rep.* **24**, 973–986.e8 (2018).
40. L. Dayon *et al.*, Alzheimer disease pathology and the cerebrospinal fluid proteome. *Alzheimers Res. Ther.* **10**, 66 (2018).
41. M. Grapp *et al.*, Choroid plexus transcytosis and exosome shuttling deliver folate into brain parenchyma. *Nat. Commun.* **4**, 2123 (2013).
42. T. C. Ma, K. I. Vong, K. M. Kwan, Spatiotemporal decline of BMP signaling activity in neural progenitors mediates fate transition and safeguards neurogenesis. *Cell Rep.* **30**, 3616–3624.e4 (2020).
43. V. Silva-Vargas, A. R. Maldonado-Soto, D. Mizrak, P. Codega, F. Doetsch, Age-dependent niche signals from the choroid plexus regulate adult neural stem cells. *Cell Stem Cell* **19**, 643–652 (2016).
44. M. P. Lun *et al.*, Spatially heterogeneous choroid plexus transcriptomes encode positional identity and contribute to regional CSF production. *J. Neurosci.* **35**, 4903–4916 (2015).Corrected in: *J. Neurosci.* **35**, 8686 (2015).
45. T. Ohyama, A. K. Groves, Generation of Pax2-Cre mice by modification of a Pax2 bacterial artificial chromosome. *Genesis* **38**, 195–199 (2004).
46. H. Akiyama, M. C. Chaboissier, J. F. Martin, A. Schedl, B. de Crombrugghe, The transcription factor Sox9 has essential roles in successive steps of the chondrocyte differentiation pathway and is required for expression of Sox5 and Sox6. *Genes Dev.* **16**, 2813–2828 (2002).
47. P. Soriano, Generalized lacZ expression with the ROSA26 Cre reporter strain. *Nat. Genet.* **21**, 70–71 (1999).
48. A. Ben-Zvi *et al.*, Mfsd2a is critical for the formation and function of the blood-brain barrier. *Nature* **509**, 507–511 (2014).